



HAL
open science

Spatiotemporal changes in substantia nigra neuromelanin content in Parkinson's disease

Emma Biondetti, Rahul Gaurav, Lydia Yahia-Cherif, Graziella Mangone, Nadya Pyatigorskaya, Romain Valabrègue, Claire Ewencyk, Matthew Hutchison, Chantal François, Isabelle Arnulf, et al.

► To cite this version:

Emma Biondetti, Rahul Gaurav, Lydia Yahia-Cherif, Graziella Mangone, Nadya Pyatigorskaya, et al.. Spatiotemporal changes in substantia nigra neuromelanin content in Parkinson's disease. *Brain - A Journal of Neurology* , 2020, 143 (9), pp.2757-2770. 10.1093/brain/awaa216 . hal-04523953

HAL Id: hal-04523953

<https://hal.sorbonne-universite.fr/hal-04523953>

Submitted on 27 Mar 2024




HAL is a multi-disciplinary open access archive for the deposit and dissemination of scientific research documents, whether they are published or not. The documents may come from teaching and research institutions in France or abroad, or from public or private research centers.

L'archive ouverte pluridisciplinaire **HAL**, est destinée au dépôt et à la diffusion de documents scientifiques de niveau recherche, publiés ou non, émanant des établissements d'enseignement et de recherche français ou étrangers, des laboratoires publics ou privés.



Distributed under a Creative Commons Attribution - NonCommercial 4.0 International License

Spatiotemporal changes in substantia nigra neuromelanin content in Parkinson's disease

 Emma Biondetti,^{1,2,3}
 Rahul Gaurav,^{1,2,3} Lydia Yahia-Cherif,^{1,2} Graziella Mangone,^{1,4}
 Nadya Pyatigorskaya,^{1,3,5} Romain Valabrègue,^{1,2} Claire Ewencyk,^{1,3,6} Matthew Hutchison,⁷ Chantal François,¹ Isabelle Arnulf,^{1,3,8} Jean-Christophe Corvol,^{1,4,6} Marie Vidailhet^{1,3,6} and Stéphane Lehéricy^{1,2,3,5}

See Vaillancourt and Mitchell (doi:10.1093/brain/awaa252) for a scientific commentary on this article.

This study aimed to investigate the spatiotemporal changes in neuromelanin-sensitive MRI signal in the substantia nigra and their relation to clinical scores of disease severity in patients with early or progressing Parkinson's disease and patients with idiopathic rapid eye movement sleep behaviour disorder (iRBD) exempt of Parkinsonian signs compared to healthy control subjects. Longitudinal T₁-weighted anatomical and neuromelanin-sensitive MRI was performed in two cohorts, including patients with iRBD, patients with early or progressing Parkinson's disease, and control subjects. Based on the aligned substantia nigra segmentations using a study-specific brain anatomical template, parametric maps of the probability of a voxel belonging to the substantia nigra were calculated for patients with various degrees of disease severity and controls. For each voxel in the substantia nigra, probability map of controls, correlations between signal-to-noise ratios on neuromelanin-sensitive MRI in patients with iRBD and Parkinson's disease and clinical scores of motor disability, cognition and mood/behaviour were calculated. Our results showed that in patients, compared to the healthy control subjects, the volume of the substantia nigra was progressively reduced for increasing disease severity. The neuromelanin signal changes appeared to start in the posterolateral motor areas of the substantia nigra and then progressed to more medial areas of this region. The ratio between the volume of the substantia nigra in patients with Parkinson's disease relative to the controls was best fitted by a mono-exponential decay. Based on this model, the pre-symptomatic phase of the disease started at 5.3 years before disease diagnosis, and 23.1% of the substantia nigra volume was lost at the time of diagnosis, which was in line with previous findings using post-mortem histology of the human substantia nigra and radiotracer studies of the human striatum. Voxel-wise patterns of correlation between neuromelanin-sensitive MRI signal-to-noise ratio and motor, cognitive and mood/behavioural clinical scores were localized in distinct regions of the substantia nigra. This localization reflected the functional organization of the nigrostriatal system observed in histological and electrophysiological studies in non-human primates (motor, cognitive and mood/behavioural domains). In conclusion, neuromelanin-sensitive MRI enabled us to assess voxel-wise modifications of substantia nigra's morphology *in vivo* in humans, including healthy controls, patients with iRBD and patients with Parkinson's disease, and identify their correlation with nigral function across all motor, cognitive and behavioural domains. This insight could help assess disease progression in drug trials of disease modification.

- 1 Institut du Cerveau – ICM, INSERM U 1127, CNRS UMR 7225, Sorbonne Université, Paris, France
- 2 ICM, Centre de NeuroImagerie de Recherche – CENIR, Paris, France
- 3 ICM, Team “Movement Investigations and Therapeutics” (MOVIT), Paris, France
- 4 National Institute of Health and Medical Research - INSERM, Clinical Investigation Centre, Pitié-Salpêtrière Hospital, Paris, France
- 5 Department of Neuroradiology, Pitié-Salpêtrière Hospital, Public Assistance - Paris Hospitals (AP-HP), Paris, France
- 6 Department of Neurology, Pitié-Salpêtrière Hospital, Public Assistance - Paris Hospitals (AP-HP), Paris, France
- 7 Biogen Inc., Cambridge, MA, USA
- 8 Sleep Disorders Unit, Pitié-Salpêtrière Hospital, Public Assistance – Paris Hospitals (AP-HP), Paris, France

Received February 25, 2020. Revised April 11, 2020. Accepted May 08, 2020. Advance access publication August 28, 2020

© The Author(s) (2020). Published by Oxford University Press on behalf of the Guarantors of Brain.

This is an Open Access article distributed under the terms of the Creative Commons Attribution Non-Commercial License (<http://creativecommons.org/licenses/by-nc/4.0/>), which permits non-commercial re-use, distribution, and reproduction in any medium, provided the original work is properly cited. For commercial re-use, please contact journals.permissions@oup.com

Correspondence to: Emma Biondetti, PhD
 Centre de NeuroImagerie de Recherche – CENIR, Institut du Cerveau – ICM, Hôpital Pitié-Salpêtrière, 47 Boulevard de l'Hôpital, 75651 Paris Cedex 13, France
 E-mail: emma.biondetti@icm-institute.org

Keywords: parkinsonism; rapid eye movement sleep behaviour disorder; substantia nigra; MRI; neuromelanin

Abbreviations: DAT = dopamine transporter; iRBD = idiopathic rapid eye movement sleep behaviour disorder; SN = substantia nigra; SNR = signal-to-noise ratio.

Introduction

Parkinson's disease is characterized by the progressive degeneration of the dopaminergic nigrostriatal system, involving the loss of neuromelanin-containing neurons in the substantia nigra (SN). Parkinson's disease can be heralded by prodromal symptoms, e.g. idiopathic rapid eye movement sleep behaviour disorder (iRBD), but is currently diagnosed after 30–50% of dopaminergic neurons in the SN are lost (Greffard *et al.*, 2006; Cheng *et al.*, 2010). By binding iron, the neuromelanin pigments in the SN dopamine neurons form paramagnetic neuromelanin-iron complexes (Sulzer *et al.*, 2018), thus enabling neuromelanin-sensitive MRI. This technique exploits the magnetization transfer effect to produce magnetic resonance images on which the SN appears hyperintense (Sulzer *et al.*, 2018). Previous studies (Sasaki *et al.*, 2006; Schwarz *et al.*, 2011; Kitao *et al.*, 2013; Ohtsuka *et al.*, 2013; Castellanos *et al.*, 2015; Langley *et al.*, 2015, 2016; Reimao *et al.*, 2015, 2016; Isaias *et al.*, 2016; Kuya *et al.*, 2016; Matsuura *et al.*, 2016; Huddleston *et al.*, 2017; Schwarz *et al.*, 2017; Ariz *et al.*, 2019; Pyatigorskaya *et al.*, 2018; Takahashi *et al.*, 2018a, b; Taniguchi *et al.*, 2018; Wang *et al.*, 2018, 2019; Xing *et al.*, 2018; Matsusue *et al.*, 2019) have used this technique to assess SN neuron density by measuring the signal intensity on neuromelanin-sensitive MRI in the visible SN relative to a background region of interest (Sasaki *et al.*, 2006; Schwarz *et al.*, 2011; Kitao *et al.*, 2013; Ohtsuka *et al.*, 2013; Langley *et al.*, 2015; Isaias *et al.*, 2016; Matsuura *et al.*, 2016; Huddleston *et al.*, 2017; Ariz *et al.*, 2019; Pyatigorskaya *et al.*, 2018; Takahashi *et al.*, 2018b; Wang *et al.*, 2018, 2019; Xing *et al.*, 2018; Matsusue *et al.*, 2019); and SN morphology by measuring the area or volume of the visible SN (Schwarz *et al.*, 2011, 2017; Castellanos *et al.*, 2015; Langley *et al.*, 2015, 2016; Reimao *et al.*, 2015, 2016; Isaias *et al.*, 2016; Kuya *et al.*, 2016; Matsuura *et al.*, 2016; Pyatigorskaya *et al.*, 2018; Takahashi *et al.*, 2018a; Taniguchi *et al.*, 2018; Wang *et al.*, 2018, 2019; Xing *et al.*, 2018; Matsusue *et al.*, 2019). Both the SN average signal intensity and size were significantly reduced in Parkinson's disease compared to healthy control subjects (Sasaki *et al.*, 2006; Schwarz *et al.*, 2011, 2017; Kitao *et al.*, 2013; Ohtsuka *et al.*, 2013; Castellanos *et al.*, 2015; Reimao *et al.*, 2015; Isaias *et al.*, 2016; Matsuura *et al.*, 2016; Huddleston *et al.*, 2017; Ariz *et al.*, 2019; Pyatigorskaya *et al.*, 2018; Takahashi *et al.*, 2018a, b; Taniguchi *et al.*, 2018; Wang *et al.*, 2018, 2019;

Matsusue *et al.*, 2019). However, previous studies have only analysed global or regional changes (e.g. in the medial, central and lateral SN) in SN neuron density and morphology. Here, we performed a voxel-wise analysis of longitudinal neuromelanin-sensitive MRI data from patients with iRBD and Parkinson's disease by aligning each subject with a study-specific brain template. First, we aimed to evaluate the local spatiotemporal variations in the SN volume. Second, because distinct areas of the SN project to distinct regions of the nigrostriatal system (Haber, 2003), we aimed to evaluate correlations between voxel-wise signal-to-noise ratios (SNRs) and motor, cognitive and behavioural clinical scores.

Materials and methods

Participants

Two cohorts were prospectively investigated, including healthy control subjects, patients with iRBD and patients with Parkinson's disease. For inclusion, patients had to be clinically diagnosed with iRBD or Parkinson's disease by a movement disorder specialist, have an age between 18 and 75 years, and have minimal or no cognitive disturbances (i.e. a Mini-Mental State Examination score >24) (Folstein *et al.*, 1975). Patients with Parkinson's disease met the UK Parkinson's Disease Society Brain Bank criteria (Hughes *et al.*, 1992). Patients with iRBD met the international diagnostic criteria for RBD, including a history of dream enactment with injurious or potentially injurious movements and the presence of enhanced tonic chin muscle tone during REM sleep (American Academy of Sleep Medicine, 2014). Idiopathic RBD was defined after a complete interview and neurological and cognitive examinations conducted by sleep neurologists due to the absence of definite criteria for parkinsonism (Hughes *et al.*, 1992).

The 'early' cohort included 38 control subjects, 42 patients with iRBD and 99 patients with early Parkinson's disease, i.e. with a disease duration <4 years, recruited between May 2015 and January 2019. In addition to the baseline examination (V1), 16 iRBD patients and 51 patients with Parkinson's disease in the early cohort underwent a follow-up examination (V2). The 'progressing' cohort included 27 controls and 30 patients with more advanced Parkinson's disease recruited between April 2010 and September 2012. In the progressing cohort, 27 Parkinson's disease patients also underwent V2.

The institutional ethical standard committee reviewed and approved both studies (CPP Paris VI/RCB: 2009-A00922-55 and RCB: 2014-A00725-42). All participants gave written informed consent.

Clinical, neurological and neuropsychological examination

All participants underwent clinical, neurological and neuropsychological examinations. In all patients and the early cohort's healthy control subjects, the severity of symptoms associated with Parkinson's disease was assessed using the Hoehn and Yahr staging scale (Hoehn and Yahr, 1967). As two distinct raters (M.V. and G.M.) had initially assessed the Hoehn and Yahr scores in the two cohorts, they then jointly performed a *post hoc* revision agreeing on the score values reported in this study. Motor disability was assessed using the Movement Disorder Society Unified Parkinson's Disease Rating Scale (MDS-UPDRS) (Goetz *et al.*, 2008) part III (early cohort) or the UPDRS (Fahn and Elton, 1987) part III (progressing cohort). Both these tests were performed 12 h after dopaminergic treatment withdrawal (OFF condition) (Goetz *et al.*, 2008). In the progressing cohort, the UPDRS-III scores were converted into MDS-UPDRS-III (Goetz *et al.*, 2012). In the early cohort, rigidity, bradykinesia and tremor subscores were also calculated (Supplementary material).

For all subjects, global cognition was assessed using the Mattis Dementia Rating Scale (DRS) (Mattis *et al.*, 1976; Mattis, 1988) including five subscores in the areas of attention, initiation, construction, conceptualization, and memory. In the early cohort, cognitive impairment was also assessed using the Montréal Cognitive Assessment (MoCA) score (Nasreddine *et al.*, 2005). Behaviour and mood were assessed using the Ardouin Scale of Behaviour in Parkinson's Disease (ASBPD) (Ardouin *et al.*, 2009; Rieu *et al.*, 2015) including 21 subscores evaluating: (i) general psychic aspects (i.e. depressive mood, hypomanic mood, anxiety, irritability and aggressiveness); (ii) apathy in behavioural terms (i.e. activity, cognitive and emotional); (iii) non-motor fluctuations, i.e. the psychological state associated with the motor symptoms in the OFF and ON states in fluctuating patients; and (iv) hyperdopaminergic behavioural disorders induced by dopaminergic treatment (i.e. nocturnal hyperactivity, diurnal somnolence, eating behaviour, creativity, hobbyism, punning, risk-taking behaviour, compulsive shopping, pathological gambling, hypersexuality, dopaminergic addiction and excess in motivation).

MRI data acquisition

All subjects were scanned on Siemens 3 T MRI systems (Siemens Healthineers): a Prisma system using a 64-channel head coil (early cohort) or a Trio system using a 32-channel head coil (progressing cohort). The MRI experiment included: a whole-brain T₁-weighted 3D acquisition for anatomical reference acquired using a magnetization-prepared two rapid gradient echo protocol (MP2RAGE in the early cohort) (Marques *et al.*, 2010) or a magnetization-prepared rapid acquisition gradient echo protocol (MPRAGE in the progressing cohort) (Mugler and Brookeman, 1991); and a T₁-weighted 2D turbo spin-echo (TSE) protocol for neuromelanin-sensitive imaging (Sulzer *et al.*, 2018) with a field of view restricted to the mid-brain. For the TSE acquisition, the transverse slices were oriented perpendicular to the long axis of the brainstem, and the field of view included both the SN and the locus coeruleus. The parameters of the MRI protocols are reported in Supplementary Table 1.

Image analysis

All analyses were carried out using MATLAB (R2017b, The MathWorks, Natick, MA, USA). Image co-registrations were performed using NiftyReg (v1.5.58). Region of interest segmentations were delineated using the FreeSurfer image viewer (v5.3.0).

For each subject, brain extraction and three-class (grey matter, white matter and CSF) tissue segmentation of the combined MP2RAGE (Marques *et al.*, 2010) (early cohort) or MPRAGE image (progressing cohort) were performed using the Computational Anatomy Toolbox (CAT12.1) for the Statistical Parametric Mapping software for MATLAB (SPM12). Moreover, the TSE image was aligned to the MP2RAGE/MPRAGE image using a block-matching affine registration algorithm (Ourselin *et al.*, 2001).

For each subject, the SN was manually segmented on the neuromelanin-sensitive image as the hyperintense area dorsal to the cerebral peduncle and ventral to the red nucleus (Pyatigorskaya *et al.*, 2017). SN segmentation was performed by two trained raters (R.G. and S.L.) blind to each subject's clinical status. For longitudinal data, SN segmentation was performed by comparing side-by-side the baseline and follow-up images. A background region of interest was drawn, including the tegmentum and superior cerebellar peduncles, to enable calculating SNRs on the TSE images.

A template of the average brain was calculated, to enable anatomical alignment of all TSE images and SN segmentations for voxel-wise analysis. Other studies on Parkinson's disease (Langley *et al.*, 2015, 2016; Huddleston *et al.*, 2017; Schwarz *et al.*, 2017) have used a similar approach by aligning individual neuromelanin-sensitive magnetic resonance images with the Montréal Neurological Institute 152 (MNI152) template, which is based on the images of a normative young adult population with an 18–90 years age range (Mazziotta *et al.*, 1995, 2001a, b). However, in a population of iRBD or Parkinson's disease patients characterized by progressive SN atrophy, the MNI152 might not best represent the average brain. Indeed, MNI152's authors suggested the need for additional templates representative of disease state, e.g. in Alzheimer's disease, traumatic brain injury, or multiple sclerosis (Mazziotta *et al.*, 2001a).

All subject populations were equally represented in the template with the same number of subjects as in the smallest group (i.e. controls), to avoid introducing a bias towards controls or patients in the TSE-to-template alignment step (Douaud *et al.*, 2007). To avoid representing twice in the template the brain anatomy of subjects scanned at both V1 and V2, longitudinal data were excluded from the template calculation. Following these considerations and because iRBD patients were only part of the early cohort, the template was calculated based on the skull stripped MP2RAGE images of 38 controls, 38 iRBD patients and 38 patients with early Parkinson's disease in the early cohort at baseline. A left-right symmetric brain template was calculated using NiftyReg and 5 affine (Ourselin *et al.*, 2001) plus 10 non-linear registration steps (Modat *et al.*, 2010) on the original and right-left flipped anatomical images. The subjects used for the template calculation were inherently co-registered to the final brain template. For all of the other subjects, the MP2RAGE/MPRAGE image was aligned to the brain template using NiftyReg and the concatenation of one affine (Ourselin *et al.*, 2001) and one non-linear transformation (Modat *et al.*, 2010).

Table 1 Demographic and clinical characteristics of the cohorts

	Early cohort					Progressing cohort				
	Healthy controls		iRBD		Parkinson's disease		HCs		Parkinson's disease	
	V1	V1	V2	V1	V2	V1	V1	V2		
Subjects, <i>n</i>	38	42	16	99	53	23	41	26		
Age, years	59.9 ± 9.3	67.7 ± 5.2 [#]	69.3 ± 4.9	61.8 ± 9.4	63.7 ± 9.1	59.7 ± 8.3	61.1 ± 9.4	63.1 ± 10.0		
Sex, M/F	17/21	37/5 [#]	13/3	66/33	31/22	12/11	27/14	16/10		
Time from V1, years	–	–	2.1 ± 0.1	–	2.1 ± 0.1	–	–	2.3 ± 0.5		
Disease duration, years	–	–	0.7 ± 0.1 (2 iRBDs)	1.5 ± 1.1	3.7 ± 1.1	–	9.9 ± 3.9	12.0 ± 3.3 (<i>n/a</i> = 2)		
Hoehn and Yahr Stage	0.1 ± 0.6	0.8 ± 1.0*	1.2 ± 1.0	2.0 ± 0.2 [#]	2.0 ± 0.2	<i>n/a</i>	2.0 ± 0.6 (<i>n/a</i> = 1)	2.2 ± 0.4		

Values are means ± standard deviations. HCs = healthy controls; *n/a* = number of subjects for which the information was unavailable.

**P* < 0.05 and

[#]*P* < 0.001 denote significant differences between iRBDs or PDs at V1 and the corresponding healthy controls at V1.

For each subject, both the SN and background regions of interest were aligned to the corresponding MP2RAGE/MPRAGE image by applying the previously calculated TSE-to-MP2RAGE/MPRAGE transformation. To mitigate potential CSF partial volume effects caused by the different resolutions of the TSE and MP2RAGE/MPRAGE images (Supplementary Table 1), all voxels in the co-registered regions of interest and having a probability of being CSF ≥ 0.05 were removed from the regions of interest. The partial volume-corrected regions of interest were then co-registered to the brain template by applying the previously calculated MP2RAGE/MPRAGE-to-template transformation.

As the controls in the two cohorts shared similar demographic and clinical characteristics (Tables 1 and 2), they were grouped to obtain a larger sample size of controls for enhanced statistical power in the following analyses. For each group of controls and patients, the average SN region of interest was calculated, which corresponded to a probability map of each voxel belonging to the SN. Then, the average SN volume of control subjects was calculated to provide a reference value against which to compare the SN volume of individual patients. To this aim, the SN probability map of controls was thresholded at a minimum value empirically set to 0.3, as the cumulative distribution function of the SN probability map of controls was approximately linear for values in the 0.3–1 range (Supplementary Fig. 1). This suggests that, for values in this range, the SN probability map reflected the true variability of the SN anatomy in controls (assumed to have a uniform histogram, as no variation in SN volume is expected) while minimizing the variability induced by inaccuracies in the manual segmentation or image co-registration steps. For each patient, the SN volume (in mm³) was calculated as the number of voxels in the manual SN segmentation aligned with the brain template (1-mm isotropic resolution). In each patient, the per cent SN volume ratio relative to controls was calculated as the ratio of the SN volume to the average SN volume in controls multiplied by 100. The per cent ratio in SN volume of individual Parkinson's disease patients was then modelled against disease duration, with $y(x)$ denoting the SN volume ratio and x the disease duration. The pre-symptomatic phase of disease was calculated by extrapolating the value of the exponential fitting curve at the point of no loss in SN volume [i.e. $y(x) = 100\%$]. The loss in SN volume at the time of disease diagnosis was calculated as the zero-intercept (i.e. $x = 0$) of the exponential fitting curve.

For each voxel, the relationship between the SNR measured on neuromelanin-sensitive MRI and each clinical score was evaluated. For this analysis, to avoid introducing a bias linked to intra-subject correlation, only the images acquired at V1 were considered. The thresholded and binarized SN region of interest calculated from the individual SN region of interest of all controls served as the reference SN volume where to calculate the voxel-wise SNR of neuromelanin-sensitive MRI. To obtain a reference background region of interest for SNR calculation, first, the background regions of interest of all controls were averaged. Then, because it was expected that the background region of interest had a similar shape and a similar signal intensity distribution across subjects, the average background region of interest was thresholded at 0.5 (i.e. the highest-uncertainty probability value, corresponding to a lack of assumptions) and binarized. For each subject at V1, the voxel-wise SNR of neuromelanin-sensitive MRI was calculated as the ratio between the neuromelanin-sensitive MRI signal intensity in the voxel and the average signal intensity in the reference background region of interest.

Statistical analysis

Statistical analyses of demographic and clinical characteristics were performed using R (v3.6.1, R Core Team, 2017) and MATLAB. All between-group comparisons of clinical and demographic variables were performed using the parametric Student's *t*-test except for intergroup differences in gender distribution, which were assessed using Pearson's χ^2 test with Yates' continuity correction.

Voxel-wise Pearson's correlation coefficients were calculated between the SNR of neuromelanin-sensitive MRI and each motor, cognitive and behavioural clinical score and subscore (Table 2), to investigate the relationship between the spatial pattern of dopaminergic neuron loss in the SN and motor, cognitive, and behavioural patient status. Because both biological sex and age influence the phenotypical expression of Parkinson's disease (Prange et al., 2019) and neuromelanin accumulates in the SN with healthy ageing (Zecca et al., 2004), patient sex and age were included as covariates of no interest in the correlation analysis. Based on a preliminary investigation on control subjects, considering the type of MRI scanner as a covariate of no interest was unnecessary (Supplementary material). The *P*-values

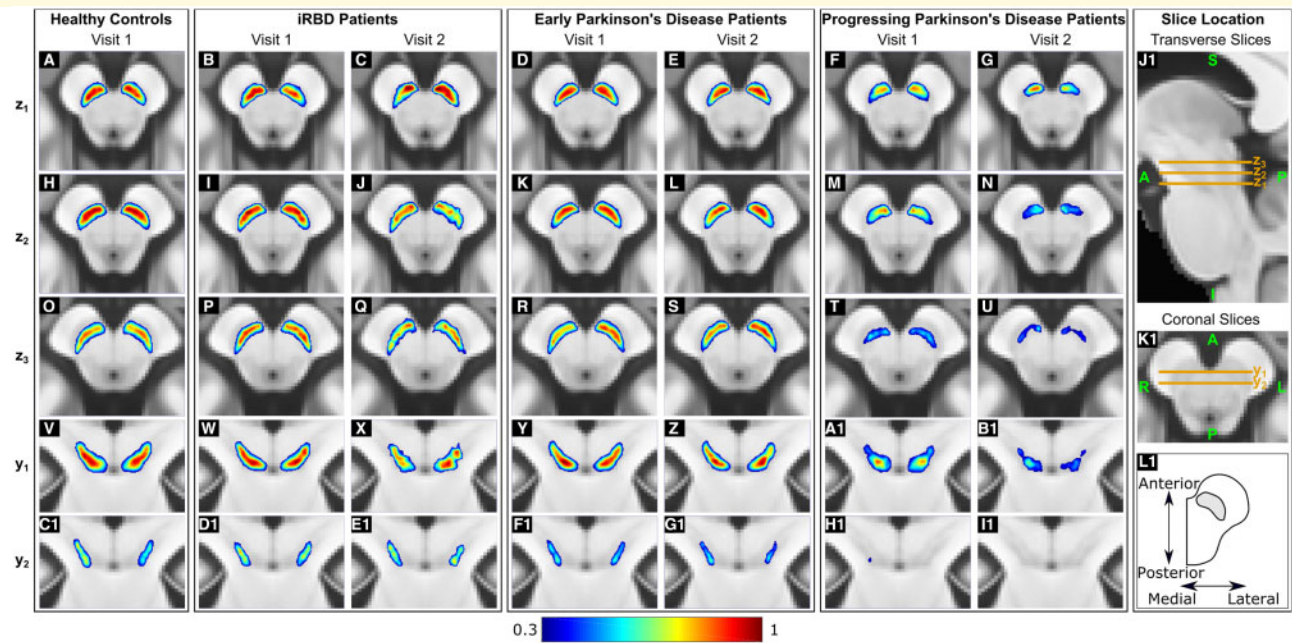


Figure 1 SN probability maps for each group of subjects. For each group of subjects, the figure shows the same three transverse slices (A–U) and the same two coronal slices (V–II) of the SN probability map overlaid on the brain template. In each image, the brain template is displayed using the same intensity range in arbitrary units. The side panels show the location of each slice (J1–K1) and the anatomical coordinates relative to the transverse slice orientation (L1). All images are displayed using the radiological convention, i.e. with the subject's right side on the left side of the image. For improved image visualization quality, the SN probability maps were spatially upsampled by a factor of 4 using nearest-neighbour interpolation.

of the correlation analysis were adjusted for comparisons across multiple voxels and multiple clinical scores using an approximate multivariate permutation test (Nichols and Holmes, 2002).

Data availability

The data supporting the findings of this study are available from the corresponding author upon reasonable request.

Results

Demographic and clinical characteristics

Tables 1 and 2 summarize the demographic and clinical characteristics of all subjects. The clinical score measurements are only reported at baseline, as the follow-up visit was excluded from the SNR versus clinical score correlation analysis. In all subjects, the clinical scores were measured on the same day as neuroimaging. Because of the unavailability of the MRI scanner on the day of the medical examination, four iRBD patients and nine patients with early Parkinson's disease underwent MRI within 3 months after clinical score measurement.

No significant differences in age and gender were observed between patients and controls except for the iRBD patients at baseline (Table 1).

In the early cohort, both patient groups at baseline had a higher MDS-UPDRS-III OFF score compared to controls (Table 2). In the progressing cohort, Parkinson's disease patients had a significantly higher UPDRS-III OFF score (30.3 ± 9.1) than controls (0.7 ± 1.0 , $P < 0.001$).

In the early cohort, both patient groups had significantly lower MoCA scores than controls (Table 2).

In the early cohort, iRBD patients had a significantly lower Mattis DRS total score than controls due to the significant decrease in the initiation and memory subscores (Table 2), and Parkinson's disease patients had a significantly lower Mattis DRS memory subscore than controls (Table 2). In the progressing cohort, patients had a significantly lower Mattis DRS total score than controls, with a significant decrease in the attention and memory subscores (Table 2).

In the early cohort, both patient groups had significantly higher total ASBPDP hypodopaminergic scores than controls due to the significant increase in the apathy subscore (Table 2). Moreover, the increased ASBPDP hypodopaminergic score of early Parkinson's disease patients was also associated with the significant increase in the depressive mood, irritability and aggressiveness, hypermotivity and psychotic symptoms subscores (Table 2). Additionally, early

Table 2 Clinical characteristics of the cohorts at baseline

	Early cohort			Progressing cohort	
	Healthy controls	iRBD patients	PD patients	Healthy controls	PD patients
MDS-UPDRS-III OFF total /subscores:	5.8 ± 5.9 (n/a = 1)	11.9 ± 6.3 [#]	30.5 ± 7.9 [#]	n/a	38.8 ± 10.8 (n/a = 1)
Rigidity	0.6 ± 0.9	1.9 ± 1.7 [#]	6.3 ± 2.4 [#]	–	n/a
Bradykinesia	2.7 ± 3.3	5.2 ± 3.5 [*]	13.0 ± 4.4 [#]	–	n/a
Tremor	1.3 ± 1.9	2.6 ± 1.9 [*]	6.1 ± 3.2 [#]	–	n/a
MoCA total	28.2 ± 1.4	27.3 ± 2.2 [*]	27.4 ± 2.3 [*]	n/a	n/a
Mattis DRS total/subscores:	140.4 ± 3.1	137.7 ± 5.8 [*]	139.0 ± 4.4 (n/a = 2)	140.0 ± 2.6	137.3 ± 4.5 [*]
Attention	36.3 ± 0.9	36.3 ± 1.0	36.0 ± 1.0	36 ± 1.2	35.4 ± 1.2 [*]
Initiation	35.8 ± 2.3	34.5 ± 3.4 [*]	35.6 ± 2.8	36.3 ± 1.7	35.4 ± 3.0
Construction	6.0 ± 0.0	6.0 ± 0.0	6.0 ± 0.2	6.0 ± 0.0	6.0 ± 0.0
Conceptualization	38.2 ± 1.3	37.5 ± 2.6	38.0 ± 1.7	37.1 ± 1.8	37.3 ± 1.8
Memory	24.1 ± 1.0	23.4 ± 1.5 [*]	23.5 ± 1.7 [*]	24.4 ± 0.8	23.0 ± 1.8 [*]
ASBPD hypodopaminergic total/subscores:	0.6 ± 0.9	1.9 ± 2.6 [*]	2.0 ± 2.0 [#] (n/a = 1)	n/a	5.2 ± 3.3
Depressive mood	0.1 ± 0.3	0.4 ± 0.8	0.3 ± 0.6 [*]	–	0.9 ± 0.9
(Hypo)maniac mood	0.3 ± 0.5	0.4 ± 0.7	0.5 ± 0.8	–	0.2 ± 0.4
Anxiety	0.0 ± 0.2	0.0 ± 0.2	0.0 ± 0.1	–	0.9 ± 1.0
Irritability and aggressiveness	0.0 ± 0.2	0.2 ± 0.5	0.2 ± 0.4 [*]	–	0.7 ± 0.9
Hyperemotivity	0.2 ± 0.4	0.6 ± 0.6	0.6 ± 0.7 [*]	–	0.6 ± 0.9
Psychotic symptoms	0.0 ± 0.0	0.1 ± 0.3	0.2 ± 0.4 [*]	–	0.4 ± 0.6
Apathy	0.0 ± 0.2	0.4 ± 0.7 [*]	0.3 ± 0.5 [*]	–	0.5 ± 0.7
Non-motor fluctuations OFF	0.0 ± 0.0	0.0 ± 0.0	0.0 ± 0.1	–	0.9 ± 0.9
ASBPD hyperdopaminergic total/subscores:	0.0 ± 0.2	0.2 ± 0.6	1.0 ± 1.5 [#] (n/a = 1)	n/a	2.6 ± 2.7
Non-motor fluctuations ON	0.0 ± 0.0	0.0 ± 0.0	0.0 ± 0.1	–	0.2 ± 0.5
Nocturnal hyperactivity	0.0 ± 0.0	0.0 ± 0.0	0.0 ± 0.2	–	0.4 ± 0.8
Daytime sleepiness	0.0 ± 0.0	0.2 ± 0.6	0.5 ± 0.7 [#]	–	0.7 ± 0.7
Eating behaviour	0.0 ± 0.0	0.0 ± 0.0	0.2 ± 0.4 [*]	–	0.5 ± 0.7
Creativity	0.0 ± 0.0	0.0 ± 0.0	0.0 ± 0.1	–	0.2 ± 0.7
Hobbyism	0.0 ± 0.0	0.0 ± 0.0	0.0 ± 0.2	–	0.1 ± 0.3
Punding	0.0 ± 0.0	0.0 ± 0.0	0.0 ± 0.2	–	0.1 ± 0.5
Risky behaviour	0.0 ± 0.0	0.0 ± 0.0	0.0 ± 0.1	–	0.1 ± 0.3
Compulsive shopping	0.0 ± 0.0	0.0 ± 0.0	0.1 ± 0.3	–	0.2 ± 0.6
Pathological gambling	0.0 ± 0.0	0.0 ± 0.0	0.1 ± 0.3	–	0.1 ± 0.3
Hypersexuality	0.0 ± 0.2	0.0 ± 0.0	0.0 ± 0.2	–	0.1 ± 0.4
Dopaminergic addiction	0.0 ± 0.0	0.0 ± 0.0	0.1 ± 0.3	–	0.0 ± 0.0
Appetitive mode	0.0 ± 0.0	0.0 ± 0.0	0.0 ± 0.0	–	0.4 ± 0.7

Values are means ± standard deviations. ASBPD = Ardouin Scale of Behaviour in Parkinson's Disease; n/a = number of subjects for which the information was unavailable; PD = Parkinson's disease.

* $P < 0.05$ denotes significant differences between iRBDs or Parkinson's disease and the corresponding healthy controls.

[#] $P < 0.001$ denotes significant differences between iRBDs or Parkinson's disease and the corresponding healthy controls.

Parkinson's disease patients had a significantly higher total ASBPD hypodopaminergic score than controls with a significant increase in the daytime sleepiness and eating behaviour subscores (Table 2).

Substantia nigra probability maps and volume analysis

Unlike previous studies on non-human primates (Mogenson et al., 1980; Haber et al., 2000; Haber, 2003, 2014; Bjorklund and Dunnett, 2007; Cavalcanti et al., 2016) that refer to the dorsal/ventral medial/lateral SN in the coronal plane, we will refer to the anterior/posterior medial/lateral SN in the transverse plane (Fig. 1). Differences arising in the levels of sampling within the SN when considering coronal

or transverse planes of reference will be explained in the 'Discussion' section.

In all patients, the probabilities in the SN took values in a smaller range compared to controls, reflecting the less consistent segmentation as SN of these areas (Fig. 1). Particularly, in iRBD and early Parkinson's disease, clusters of low probability were localized in the posterolateral SN (Fig. 1). In progressing Parkinson's disease, clusters of low probability extended to medial and anterior areas of the SN, and differences compared to the other groups were easier to appreciate on visual inspection (Fig. 1). These results suggest a spatial pattern of neurodegeneration extending from the posterolateral to the anteromedial SN over the course of disease.

In Parkinson's disease patients, a mono-exponential function best fitted the SN volume ratios relative to controls

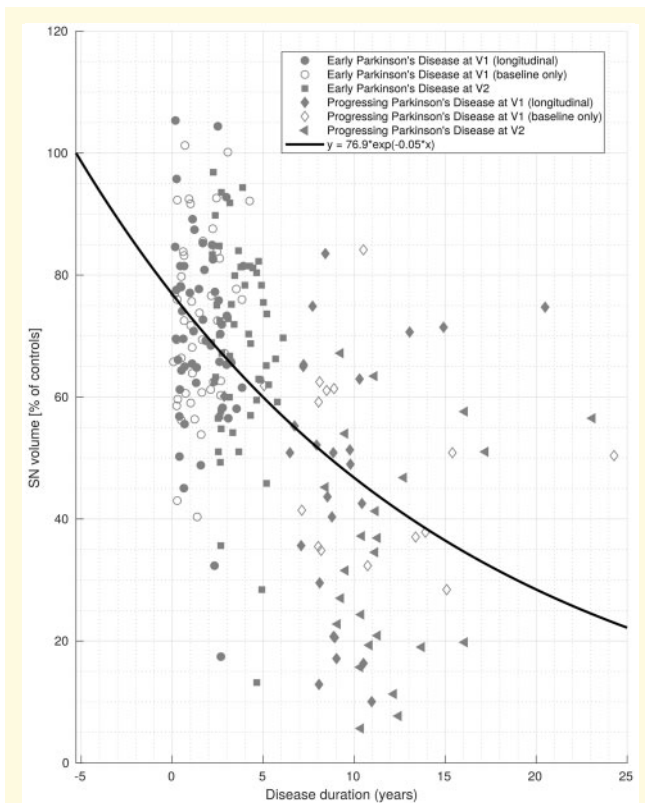


Figure 2 The temporal decrease in SN volume ratio in patients relative to controls. For all Parkinson's disease patients relative to control subjects, the individual per cent ratios of SN volume and the mono-exponential fitting function are plotted against the mean disease duration. The filled and empty markers denote the subjects with and without V2, respectively.

versus the mean disease duration (adjusted $R^2 = 0.99$, Fig. 2). Based on this model, the pre-symptomatic phase of disease [i.e. the value of disease duration at $y(x) = 100\%$ in Fig. 2] started 5.3 years before disease diagnosis, and 23.1% of the SN was lost at the time of disease diagnosis (i.e. the value of SN volume ratio at $x = 0$ in Fig. 2). In agreement with this estimation, the SN volume ratio in the iRBD patients at both baseline ($76.8 \pm 14.4\%$) and follow-up ($76.6 \pm 15.0\%$) was equal to or higher than the SN volume ratio in the early Parkinson's disease patients at baseline ($71.5 \pm 15.0\%$).

Correlation between clinical scores and the signal-to-noise ratio of neuromelanin-sensitive MRI

In the motor domain, in the bilateral posterolateral SN there was a significant negative correlation between the MDS-UPDRS-III OFF score and the neuromelanin SNR both when considering all subjects and those in the early cohort only (arrowheads in Figs 3 and 4 and Supplementary Fig. 2). In the early cohort, there was also a significant negative correlation between all three aggregated motor subscores

and the neuromelanin SNR. In particular, the bradykinesia subscore had the largest correlation pattern located in the bilateral SN, the tremor subscore had the second-largest correlation pattern mostly located in the left posterolateral SN, and the rigidity subscore was only weakly correlated (Supplementary Fig. 2).

In the cognitive domain, there was a significant positive correlation between the neuromelanin SNR and the Mattis DRS attention subscore in the anteromedial and superior SN (arrowheads in Figs 3 and 4) whereas no significant correlation was found between the neuromelanin SNR and the other Mattis DRS subscores. There was also a weak positive correlation with the total Mattis DRS score. In the early cohort, there was no significant correlation with the MoCA score.

In the mood/behaviour domain, there was a significant negative correlation between the neuromelanin SNR and both the aggregated hypodopaminergic and hyperdopaminergic scores of the ASBPD scale (Fig. 3). The neuromelanin SNR was negatively correlated with all the ASBPD subscores (Fig. 3 shows representative apathy and creativity subscores)—except pathological gambling, hypersexuality and dopaminergic addiction—in the medial areas of the SN (arrowheads in Fig. 3).

All three domains partially overlapped (Fig. 4).

Discussion

Based on neuromelanin-sensitive MRI of healthy control subjects at baseline and longitudinal neuromelanin-sensitive MRI of patients with iRBD or idiopathic Parkinson's disease, this study investigated the spatiotemporal changes in the SN in prodromal and clinical Parkinson's disease. First, the 3D voxel-based pattern of progression for SN neurodegeneration was demonstrated (Fig. 1). Then, by fitting the SN volume ratio of Parkinson's disease patients relative to controls, the SN volume ratio was shown to exponentially decrease with advancing disease duration with a pre-symptomatic phase starting 5.3 years before disease diagnosis and an estimated 23.1% loss in SN volume at the time of diagnosis (Fig. 2). Finally, by calculating voxel-wise correlations between the SNR of neuromelanin-sensitive MRI and clinical scores evaluating motor, cognitive and behavioural impairment, three territories were identified: sensorimotor in the posterolateral SN, limbic in the anteromedial SN and associative in the superior and anterior SN (Figs 3 and 4) with a significant overlap between the three territories.

A decrease in the SN volume was observed in Parkinson's disease patients relative to controls (Figs 1 and 2). At 2-year median disease duration, one study has reported a 53% average decrease in the SN volume of patients relative to controls (Schwarz *et al.*, 2017). At 6-year median disease duration, previous studies have reported an average decrease in the SN volume of $\sim 38\%$ (Castellanos *et al.*, 2015), 27% (Isaias *et al.*, 2016) or 6% (Takahashi *et al.*, 2018a) in patients relative to controls. The discrepancy between SN

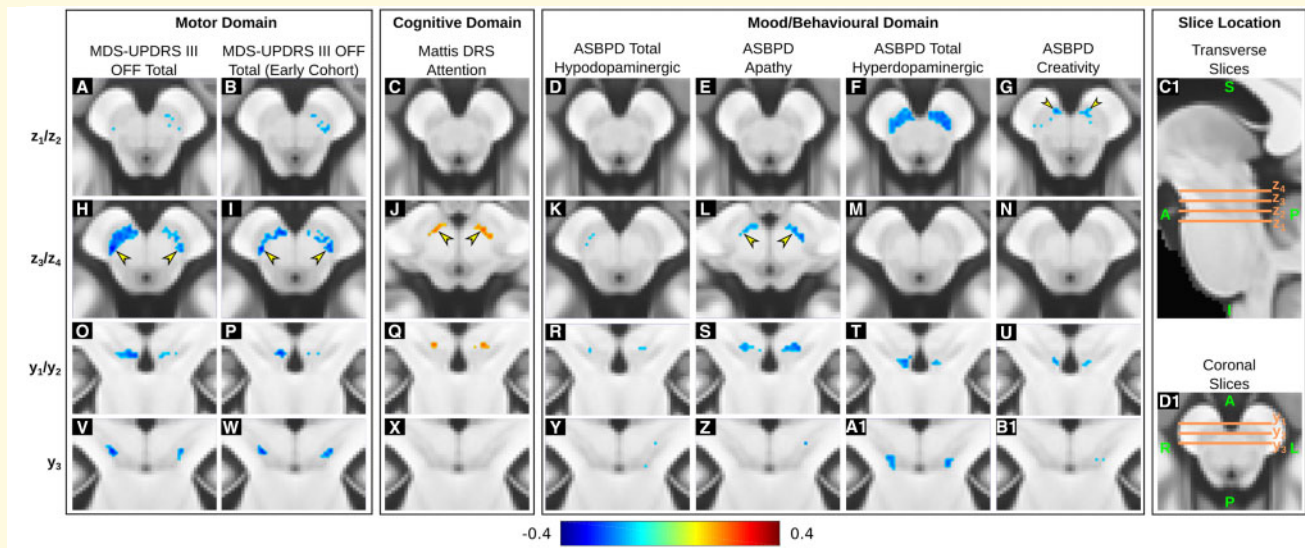


Figure 3 Voxel-wise correlations between clinical scores and the SNR of neuromelanin-sensitive MRI. For each functional domain (motor, cognitive and mood/behavioural), the same two transverse (A–N) and two coronal slices (O–I) of the most representative correlation patterns between neuromelanin SNR and clinical scores are shown overlaid on the brain template. The side panels show the location of the transverse (C1) and coronal slices (D1), respectively on the brain template. Similar to Fig. 1, all images are displayed using the radiological convention and, for improved visualization quality, the correlation maps were spatially upsampled by a factor of four using nearest-neighbour interpolation. In H–J, L and G, the yellow arrowheads point at patterns of correlation discussed in the main text.

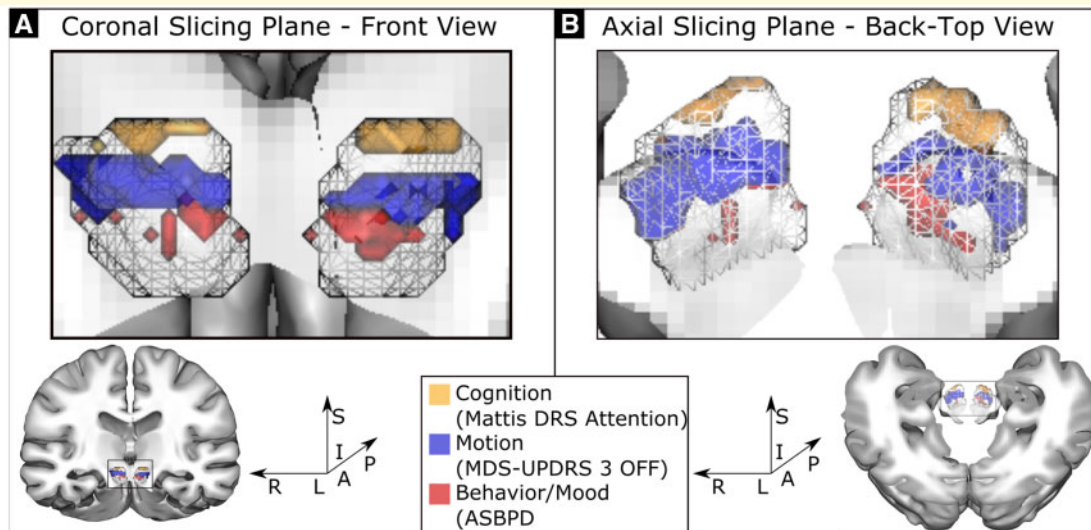


Figure 4 Three-dimensional rendering of the SN functional territories. Three-dimensional front (A) and back-top views (B) of the average SN region of interest of healthy controls and three representative SNR-clinical correlation patterns are shown against coronal (A) and axial slicing planes (B) of the brain template. For display in the figure, all patterns of correlation were thresholded at ≥ 0.01 (absolute value) and binarized. The transparency of all patterns was set to 60%, to enable visualizing potential overlaps between correlation patterns.

volume losses previously reported at 6-year disease duration could be due to the different methods used for SN segmentation: morphology-based using manual SN delineations in 16 healthy subjects and a majority voting approach for voxel classification (Castellanos *et al.*, 2015), intensity-based thresholding (Isaias *et al.*, 2016; Schwarz *et al.*, 2017), or

SNR-based thresholding (Takahashi *et al.*, 2018a). Moreover, in the study analysing 30 healthy control subjects versus 39 Parkinson's disease patients at 2 years from diagnosis (Schwarz *et al.*, 2017), the variance of the SN volume measured in controls was more than double the one measured in patients. As was suggested by the authors

(Schwarz *et al.*, 2017), the low precision of current neuromelanin-sensitive imaging methods could explain this large intergroup discrepancy in the variability of SN volume measurements. Thus, further work is needed to develop neuromelanin-sensitive MRI protocols improving measurement precision of neuromelanin signal intensity in the SN and, thus, SN volume.

Based on all groups of Parkinson's disease patients, a negative mono-exponential function best fitted the SN volume loss against mean disease duration (Fig. 2). Negative mono-exponential curves describing the temporal degeneration of the nigrostriatal system have also been reported by studies using histology for the count of pigmented cell bodies in the SN (Fearnley and Lees, 1991; Greffard *et al.*, 2006), studies using dopamine transporter (DAT) single-photon emission computed tomography (SPECT) for the assessment of striatal presynaptic dopamine neuronal function (Staffen *et al.*, 2000; Pirker *et al.*, 2003; Schwarz *et al.*, 2004; Nandhagopal *et al.*, 2009; Jakobson Mo *et al.*, 2013; Simuni *et al.*, 2018; Ikeda *et al.*, 2019), and studies using PET for the assessment of dopamine content in the striatal terminals (Hilker *et al.*, 2005; Nandhagopal *et al.*, 2009; de la Fuente-Fernandez *et al.*, 2011). These results suggest that degeneration of the nigrostriatal system in Parkinson's disease as a whole occurs at a faster rate in the early phases of disease than in later phases. In apparent contrast with this hypothesis, some studies using DAT-SPECT have reported a linear decrease in dopamine function with advancing disease duration (Chouker *et al.*, 2001; Marek *et al.*, 2001; Parkinson Study Group, 2002; Ikeda *et al.*, 2019). The discrepancy observed in these studies and the DAT-SPECT studies reporting exponential degeneration patterns could be explained by differences in the age of patients at inclusion, the number of DAT-SPECT scans performed (ranging from two to four) and the time interval between consecutive scans (ranging from 1.0 to 5.5 years). Notably, the one study using DAT-SPECT (Schwarz *et al.*, 2004) that followed patients for the longest time performing the highest number of scans (i.e. at baseline and at 1.0, 2.0 and 7.5 years from baseline) reported an exponential decline in dopamine neuronal function in agreement with our results (Fig. 2). Because a large subset of patients in the early cohort also underwent longitudinal DAT-SPECT imaging, future work will involve comparing the decline in SN volume calculated using neuromelanin-sensitive MRI with the decline in DAT binding in the striatum.

Based on the mono-exponential model of SN loss in Parkinson's disease, at the time of diagnosis, there was a 23.1% decrease in melanized neurons (Fig. 2). Here, the measured loss in SN at diagnosis was lower than the 30–50% calculated using histology-based neuronal counts (Fearnley and Lees, 1991; Greffard *et al.*, 2006; Cheng *et al.*, 2010) and slightly lower than the 30–34% reported by measuring striatal presynaptic dopamine function in patients with approximately the same age (Hilker *et al.*, 2005; Nandhagopal *et al.*, 2009; de la Fuente-Fernandez *et al.*, 2011). This discrepancy could be motivated by the

presence of extraneuronal neuromelanin deposits, which would be visible on neuromelanin-sensitive MRI, even after dopaminergic neuron death. Indeed, due to their insolubility, neuromelanin granules can remain in the extracellular space for long periods of time (Sulzer *et al.*, 2018). This phenomenon has been observed in both patients with Parkinson's disease (McGeer *et al.*, 1988) and normally ageing subjects (Beach *et al.*, 2007), and in the first rodent model of age-dependent human-like neuromelanin production in the SN pars compacta (Carballo-Carbajal *et al.*, 2019). In all these studies, the observed spatial pattern of extraneuronal neuromelanin resembled the distribution of the neuromelanin pigments when the neurons were intact. Moreover, it has recently been suggested that a progressive increase in neuromelanin in the dopaminergic neurons of the SN pars compacta could first result in neuronal dysfunction (once some threshold level in the quantity of intraneuronal neuromelanin is reached) and only trigger neuronal death at a later stage (Carballo-Carbajal *et al.*, 2019). Finally, even if manual drawing is the gold-standard method for region of interest delineation, calculating the SN volume based on manual segmentations cannot account for the potential loss of pigmented neurons within the boundaries of the hyperintense neuromelanin. Indeed, concomitant to a slight decrease in the overall delineated SN volume, there could be a decrease in the neuronal content within the boundaries of this volume. These two factors taken together could account for a 30% loss in dopaminergic neurons. However, alternative intensity-based (Isaias *et al.*, 2016; Schwarz *et al.*, 2017) or SNR-based methods (Takahashi *et al.*, 2018a) for the semi-automated segmentation of the SN require carefully choosing a segmentation threshold for the neuromelanin-sensitive image. For neuromelanin-sensitive MRI several protocols are available, some of which (including our TSE protocols) are not purely quantitative. As the choice of MRI protocol affects the SN-to-background intensity in the neuromelanin-sensitive images, making intensity-based or SNR-based segmentation approaches less easily reproducible between studies or sites, future work is needed to compare the accuracy, precision and multi-site reproducibility of such protocols.

The SN volume loss in iRBD was always equal to or lower than in Parkinson's disease, and the prodromal phase of Parkinson's disease was estimated to start 5.3 years before disease diagnosis (Fig. 2). This result was in line with the findings of a recent multicentre study on 1280 iRBD patients (Postuma *et al.*, 2019). Here, after an average follow-up time of 4.6 ± 3.5 years, 28% of patients converted to a neurodegenerative syndrome, which was parkinsonism in 56.5% of the cases. The estimated duration of the pre-symptomatic phase was also in line with histology studies reporting values of 4.7 (Fearnley and Lees, 1991) and 5.0 years (Greffard *et al.*, 2006). Notably, PET studies have reported longer pre-symptomatic phases ranging from 5.6 (Hilker *et al.*, 2005) to 10.0 years (de la Fuente-Fernandez *et al.*, 2011) supporting the hypothesis that damage to dopaminergic axons precedes cell death in the SN (Zou *et al.*, 2016).

Spatial patterns of correlation between the SNR of neuromelanin-sensitive MRI and distinct clinical scores of disease severity were localized in distinct areas of the SN (Figs 3, 4 and Supplementary Fig. 2). The localization of these correlation patterns reflected the functional organization of the nigrostriatal connections in primates (Mogenson *et al.*, 1980; Haber *et al.*, 2000; Haber, 2003, 2014; Bjorklund and Dunnett, 2007; Cavalcanti *et al.*, 2016) and rodents (Nauta *et al.*, 1978; Mogenson *et al.*, 1980; Bjorklund and Dunnett, 2007). Comparing histology-based and imaging-based results is challenging because, to section the midbrain, histology-based studies use coronally oriented planes, whereas imaging-based studies most frequently use axially oriented planes. In human studies, the SN was commonly divided into three tiers from dorsal to ventral (dorsal tier and ventral tier of pars compacta and pars reticulata) (Fearnley and Lees, 1991). In primate studies, the dorsal tier included the ventral tegmental area and the dorsal SN pars compacta, and the ventral tier included a densocellular region and cell columns extending into the SN pars reticulata (Haber *et al.*, 2000). Because of the parallel arrangement of cells in the SN and the SN oblique orientation, there was little difference in the cross-sectional configuration of the neuronal groups between the two planes (Fearnley and Lees, 1991). However, in the axial versus coronal plane, the medial groups and dorsal tier were located at a higher rostral level and the lateral groups and ventral tier at a lower caudal level (Fearnley and Lees, 1991). Here, the correlation pattern between the SNR and the MDS-UPDRS-III-OFF score of motor disability was located in the posterolateral SN at lower levels (Figs 3, 4 and Supplementary Fig. 2). This location was in agreement with the disease-related loss of cell columns receiving input from the motor and premotor cortex via the sensorimotor areas of the striatum (Haber *et al.*, 2000; Haber, 2003). This topography also corresponded to the area where dopaminergic neuronal loss was most pronounced in Parkinson's disease, i.e. in the posterolateral tier including the nigrostriatal area, the anterior tier being the most preserved (Fearnley and Lees, 1991; Damier *et al.*, 1999; Jellinger, 2012). Several studies have reported correlations between the UPDRS/MDS-UPDRS-III or Hoehn and Yahr scores and changes, within the SN, in neuromelanin (Isaias *et al.*, 2016; Kawaguchi *et al.*, 2016; Matsuura *et al.*, 2016; Schwarz *et al.*, 2017; Prasad *et al.*, 2018; Taniguchi *et al.*, 2018; Wang *et al.*, 2018), iron content measured based on the tissue apparent transverse relaxation rate $R2^*$ (Martin *et al.*, 2008; Langkammer *et al.*, 2016) or magnetic susceptibility (He *et al.*, 2015; Langkammer *et al.*, 2016; An *et al.*, 2018; Cheng *et al.*, 2019) and water diffusion metrics (Ofori *et al.*, 2015; Langley *et al.*, 2016; Burciu *et al.*, 2017; Pyatigorskaya *et al.*, 2018). Notably, in agreement with our observed large pattern of correlation between the neuromelanin SNR and the bradykinesia subscore (Supplementary Fig. 2), one study found the highest correlation between baseline free water values and longitudinal changes in the bradykinesia subscore of the MDS-UPDRS scale (Ofori *et al.*, 2015). In the early cohort, the left-lateralized correlation between

the neuromelanin SNR and the tremor subscore (Supplementary Fig. 2) could be explained by the predominance (i.e. 56%) of right-sided motor symptoms in our early Parkinson's disease cohort (Scherfler *et al.*, 2012). The novelty of our study is that it provides a 3D localization of the affected region within the SN, which corresponded to the sensorimotor territory of the SN.

The correlation patterns between the SNR and the ASBPD subscores of mood/behaviour were located in the anteromedial SN (Figs 3 and 4) in agreement with the disease-related loss of retrorubral cell groups receiving input from the orbital and medial prefrontal cortex via the limbic system (Haber *et al.*, 2000; Haber, 2003). In animals, this region is involved in processing dopamine-based reward prediction error signals and reinforcement learning (Montague *et al.*, 1996; Schultz *et al.*, 1997). In humans, blood oxygen level-dependent functional MRI studies (D'Ardenne *et al.*, 2008; Boehler *et al.*, 2011; Pauli *et al.*, 2015) have also reported that the ventral tegmental area encodes positive reward prediction error signals (D'Ardenne *et al.*, 2008; Pauli *et al.*, 2015) even in the absence of external motivating factors during tasks that require to recruit processing resources needed to meet enhanced task demands (Boehler *et al.*, 2011).

Finally, the correlation pattern between the SNR and the Mattis DRS score of cognitive impairment was located in the anteromedial SN more lateral to the ASBPD and anterior to the MDS-UPDRS-III (Figs 3 and 4) in agreement with the disease-related loss of cells in the anteromedial tier of the SN receiving input from the dorsolateral prefrontal cortex via the associative striatum in non-human primates (Haber, 2003) and in agreement with electrophysiology measurements during cognitive tasks in humans (Zaghloul *et al.*, 2009). This location was in agreement with the location of terminations from the associative striatum more lateral to the ones from the limbic system and more medial to the ones from the motor striatum (Haber, 2003).

One limitation of this study was that the early and progressing cohorts included different Parkinson's disease patients. However, as the early cohort is enrolled in an ongoing longitudinal study, future work could involve updating our results after a 5-year follow-up. A further limitation was that, in the two cohorts, images were acquired using different MRI systems from the same vendor. However, the TSE protocols for neuromelanin-sensitive MRI were only slightly different (Supplementary Table 1) and no significant effect of the scanner on the voxel-wise SNR values of neuromelanin-sensitive measurements was detected in controls (Supplementary material). Finally, the MDS-UPDRS-III OFF score of iRBD patients at baseline (i.e. 11.9 ± 6.3) could appear high for patients in a pre-parkinsonian phase. However, in the presence of phenoconversion, previous studies on iRBD have reported relatively high (i.e. >4) MDS-UPDRS-III scores (Postuma *et al.*, 2019) and have shown that motor examination signs have a faster progression 1–2 years before phenoconversion (Fereshtehnejad *et al.*, 2019). Moreover, a study stratifying iRBD patients based on the outcome of DAT-SPECT has reported that, in iRBD with or

without dopaminergic denervation, MDS-UPDRS-III scores were equal to 10.5 ± 7.5 (indicative of prodromal Parkinson's disease) and 6.0 ± 4.8 , respectively, whereas in healthy control subjects the score was equal to 3.2 ± 3.2 (Dusek *et al.*, 2019). Thus, in our iRBD cohort, the relatively high MDS-UPDRS-III score could result from most patients being close to phenoconversion.

Conclusions

Based on a voxel-based analysis of neuromelanin-sensitive MRI in a group-specific brain template, this study demonstrated that there was a progressive loss of neuromelanin in the substantia nigra from prodromal to early and progressing clinical Parkinson's disease over time. This process translated into a loss of the global volume of the substantia nigra and a voxel-specific loss in the signal-to-noise ratio measured on neuromelanin-sensitive MRI. Particularly, the loss in signal-to-noise ratio correlated with the severity of clinical symptoms in an anatomically localized fashion reflecting the functional organization of the nigrostriatal system into motor, associative and limbic-emotional areas. In clinical trials, these findings could help to develop disease-modifying therapies.

Acknowledgements

The authors would like to thank all the subjects who participated in this study.

Funding

This study was funded by grants from ANR Nucleipark, DHOS-Inserm, France Parkinson, École des NeuroSciences de Paris (ENP), Fondation pour la Recherche Médicale (FRM), and the Investissements d'Avenir, IAIHU-06 (Paris Institute of Neurosciences – IHU), ANR-11-INBS-0006, Fondation d'Entreprise EDF, Biogen Inc., Fondation Thérèse and René Planiol, Unrestricted support for Research on Parkinson's disease from Energipole (M. Mallart) and Société Française de Médecine Esthétique (M. Legrand).

Competing interests

E.B. and R.G. received grants from Biogen Inc. R.V., L.Y.-C., N.P., G.M. and C.F. have nothing to disclose. C.E. received funding from Fondation pour la Recherche Médicale (FRM). J.-C.C. received grants from Agence Nationale de la Recherche, French Ministry of Health, France Parkinson, The Michael J. Fox Foundation outside of this work; he participated to scientific advisory boards for Idorsia, Sanofi, Ever Pharma, Denali, Biogen, Air Liquide, BrainEver, Theranexus outside of this work; and he received grants from 'Investissements d'avenir' [grant number ANR-10-

IAIHU-06 and ANR-11-INBS-0006] during the conduct of the study and research grants from Biogen Inc. M.V. received grants from Fondation d'Entreprise (EDF), the Fondation Thérèse and René Planiol pour l'étude du Cerveau, Unrestricted support for Research on Parkinson's disease from Energipole (M. Mallart) and Société Française de Médecine Esthétique (M. Legrand). S.L. received grants from Agence Nationale de la Recherche (ANRMNP 2009, Nucleipark), DHOS-Inserm (2010, Nucleipark), France Parkinson (2008), École Neurosciences de Paris, 'Investissements d'avenir' [grant number ANR-10-IAIHU-06 and ANR-11-INBS-0006] during the conduct of the study and research grant from Biogen Inc.

Supplementary material

Supplementary material is available at *Brain* online.

References

- American Academy of Sleep Medicine. International classification of sleep disorders, 3rd edn. Darien, IL: American Academy of Sleep Medicine; 2014.
- An H, Zeng X, Niu T, Li G, Yang J, Zheng L, et al. Quantifying iron deposition within the substantia nigra of Parkinson's disease by quantitative susceptibility mapping. *J Neurol Sci* 2018; 386: 46–52.
- Ardouin C, Chereau I, Llorca PM, Lhommee E, Durif F, Pollak P, et al. [Assessment of hyper- and hypodopaminergic behaviors in Parkinson's disease]. *Rev Neurol (Paris)* 2009; 165: 845–56.
- Ariz M, Abad RC, Castellanos G, Martinez M, Munoz-Barrutia A, Fernandez-Seara MA, et al. Dynamic Atlas-based segmentation and quantification of Neuromelanin-rich brainstem structures in Parkinson disease. *IEEE Trans Med Imaging* 2019; 38: 813–23.
- Beach TG, Sue LI, Walker DG, Lue LF, Connor DJ, Caviness JN, et al. Marked microglial reaction in normal aging human substantia nigra: correlation with extraneuronal neuromelanin pigment deposits. *Acta Neuropathol* 2007; 114: 419–24.
- Bjorklund A, Dunnett SB. Dopamine neuron systems in the brain: an update. *Trends Neurosci* 2007; 30: 194–202.
- Boehler CN, Hopf JM, Krebs RM, Stoppel CM, Schoenfeld MA, Heinze HJ, et al. Task-load-dependent activation of dopaminergic midbrain areas in the absence of reward. *J Neurosci* 2011; 31: 4955–61.
- Burciu RG, Ofori E, Archer DB, Wu SS, Pasternak O, McFarland NR, et al. Progression marker of Parkinson's disease: a 4-year multi-site imaging study. *Brain* 2017; 140: 2183–92.
- Carballo-Carbajal I, Laguna A, Romero-Gimenez J, Cuadros T, Bove J, Martinez-Vicente M, et al. Brain tyrosinase overexpression implicates age-dependent neuromelanin production in Parkinson's disease pathogenesis. *Nat Commun* 2019; 10: 973.
- Castellanos G, Fernandez-Seara MA, Lorenzo-Betancor O, Ortega-Cubero S, Puigvert M, Uranga J, et al. Automated neuromelanin imaging as a diagnostic biomarker for Parkinson's disease. *Mov Disord* 2015; 30: 945–52.
- Cavalcanti J, Pontes ALB, Fiuza FP, Silva KDA, Guzen FP, Lucena EES, et al. Nuclear organization of the substantia nigra, ventral tegmental area and retrorubral field of the common marmoset (*Callithrix jacchus*): a cytoarchitectonic and TH-immunohistochemistry study. *J Chem Neuroanat* 2016; 77: 100–9.
- Cheng HC, Ulane CM, Burke RE. Clinical progression in Parkinson disease and the neurobiology of axons. *Ann Neurol* 2010; 67: 715–25.

- Cheng Z, Zhang J, He N, Li Y, Wen Y, Xu H, et al. Radiomic features of the Nigrosome-1 region of the Substantia Nigra: using quantitative susceptibility mapping to assist the diagnosis of idiopathic Parkinson's Disease. *Front Aging Neurosci* 2019; 11: 167.
- Chouker M, Tatsch K, Linke R, Pogarell O, Hahn K, Schwarz J. Striatal dopamine transporter binding in early to moderately advanced Parkinson's disease: monitoring of disease progression over 2 years. *Nucl Med Commun* 2001; 22: 721–5.
- D'Ardenne K, McClure SM, Nystrom LE, Cohen JD. BOLD responses reflecting dopaminergic signals in the human ventral tegmental area. *Science* 2008; 319: 1264–7.
- Damier P, Hirsch EC, Agid Y, Graybiel AM. The substantia nigra of the human brain. II. Patterns of loss of dopamine-containing neurons in Parkinson's disease. *Brain* 1999; 122: 1437–48.
- de la Fuente-Fernandez R, Schulzer M, Kuramoto L, Cragg J, Ramachandiran N, Au WL, et al. Age-specific progression of nigrostriatal dysfunction in Parkinson's disease. *Ann Neurol* 2011; 69: 803–10.
- Douaud G, Smith S, Jenkinson M, Behrens T, Johansen-Berg H, Vickers J, et al. Anatomically related grey and white matter abnormalities in adolescent-onset schizophrenia. *Brain* 2007; 130: 2375–86.
- Dusek P, Ibarburu V, Bezdicek O, Dall'antonia I, Dostalova S, Kovalska P, et al. Relations of non-motor symptoms and dopamine transporter binding in REM sleep behavior disorder. *Sci Rep* 2019; 9: 15463.
- Fahn S, Elton R, Members of the UPDRS Development Committee. Recent developments in Parkinson's disease. Florham Park, NJ: Macmillan Health Care Information; 1987.
- Fearnley JM, Lees AJ. Ageing and Parkinson's disease: substantia nigra regional selectivity. *Brain* 1991; 114: 2283–301.
- Fereshtehnejad SM, Yao C, Pelletier A, Montplaisir JY, Gagnon JF, Postuma RB. Evolution of prodromal Parkinson's disease and dementia with Lewy bodies: a prospective study. *Brain* 2019; 142: 2051–67.
- Folstein MF, Folstein SE, McHugh PR. "Mini-mental state". *J Psychiatr Res* 1975; 12: 189–98.
- Goetz CG, Stebbins GT, Tilley BC. Calibration of unified Parkinson's disease rating scale scores to Movement Disorder Society-unified Parkinson's disease rating scale scores. *Mov Disord* 2012; 27: 1239–42.
- Goetz CG, Tilley BC, Shaftman SR, Stebbins GT, Fahn S, Martinez-Martin P, et al. Movement Disorder Society-sponsored revision of the Unified Parkinson's Disease Rating Scale (MDS-UPDRS): scale presentation and clinimetric testing results. *Mov Disord* 2008; 23: 2129–70.
- Greffard S, Verny M, Bonnet AM, Beinis JY, Gallinari C, Meaume S, et al. Motor score of the Unified Parkinson Disease Rating Scale as a good predictor of Lewy body-associated neuronal loss in the substantia nigra. *Arch Neurol* 2006; 63: 584–8.
- Haber SN. The primate basal ganglia: parallel and integrative networks. *J Chem Neuroanat* 2003; 26: 317–30.
- Haber SN. The place of dopamine in the cortico-basal ganglia circuit. *Neuroscience* 2014; 282: 248–57.
- Haber SN, Fudge JL, McFarland NR. Striatonigrostriatal pathways in primates form an ascending spiral from the shell to the dorsolateral striatum. *J Neurosci* 2000; 20: 2369–82.
- He N, Ling H, Ding B, Huang J, Zhang Y, Zhang Z, et al. Region-specific disturbed iron distribution in early idiopathic Parkinson's disease measured by quantitative susceptibility mapping. *Hum Brain Mapp* 2015; 36: 4407–20.
- Hilker R, Schweitzer K, Coburger S, Ghaemi M, Weisenbach S, Jacobs AH, et al. Nonlinear progression of Parkinson disease as determined by serial positron emission tomographic imaging of striatal fluorodopa F 18 activity. *Arch Neurol* 2005; 62: 378–82.
- Hoehn MM, Yahr MD. Parkinsonism: onset, progression and mortality. *Neurology* 1967; 17: 427–42.
- Huddlestone DE, Langley J, Sedlacik J, Boelmans K, Factor SA, Hu XP. In vivo detection of lateral-ventral tier nigral degeneration in Parkinson's disease. *Hum Brain Mapp* 2017; 38: 2627–34.
- Hughes AJ, Daniel SE, Kilford L, Lees AJ. Accuracy of clinical diagnosis of idiopathic Parkinson's disease: a clinico-pathological study of 100 cases. *J Neurol Neurosurg Psychiatry* 1992; 55: 181–4.
- Ikedo K, Ebina J, Kawabe K, Iwasaki Y. Dopamine transporter imaging in Parkinson disease: progressive changes and therapeutic modification after anti-parkinsonian medications. *Intern Med* 2019; 58: 1665–72.
- Isaias IU, Trujillo P, Summers P, Marotta G, Mainardi L, Pezzoli G, et al. Neuromelanin imaging and dopaminergic loss in Parkinson's disease. *Front Aging Neurosci* 2016; 8: 196.
- Jakobson Mo S, Linder J, Forsgren L, Holmberg H, Larsson A, Riklund K. Pre- and postsynaptic dopamine SPECT in idiopathic Parkinsonian diseases: a follow-up study. *Biomed Res Int* 2013; 2013: 143532.
- Jellinger KA. Neuropathology of sporadic Parkinson's disease: evaluation and changes of concepts. *Mov Disord* 2012; 27: 8–30.
- Kawaguchi H, Shimada H, Kodaka F, Suzuki M, Shinotoh H, Hirano S, et al. Principal component analysis of multimodal neuromelanin MRI and dopamine transporter PET data provides a specific metric for the nigral dopaminergic neuronal density. *PLoS One* 2016; 11: e0151191.
- Kitao S, Matsusue E, Fujii S, Miyoshi F, Kaminou T, Kato S, et al. Correlation between pathology and neuromelanin magnetic resonance imaging in Parkinson's disease and dementia with Lewy bodies. *Neuroradiology* 2013; 55: 947–53.
- Kuya K, Shinohara Y, Miyoshi F, Fujii S, Tanabe Y, Ogawa T. Correlation between neuromelanin-sensitive magnetic resonance imaging and (123)I-FP-CIT SPECT in patients with parkinsonism. *Neuroradiology* 2016; 58: 351–6.
- Langkammer C, Pirpamer L, Seiler S, Deistung A, Schweser F, Franthal S, et al. Quantitative susceptibility mapping in Parkinson's disease. *PLoS One* 2016; 11: e0162460.
- Langley J, Huddlestone DE, Chen X, Sedlacik J, Zachariah N, Hu X. A multicontrast approach for comprehensive imaging of substantia nigra. *Neuroimage* 2015; 112: 7–13.
- Langley J, Huddlestone DE, Merritt M, Chen X, McMurray R, Silver M, et al. Diffusion tensor imaging of the substantia nigra in Parkinson's disease revisited. *Hum Brain Mapp* 2016; 37: 2547–56.
- Marek K, Innis R, van Dyck C, Fussell B, Early M, Eberly S, et al. [123I]beta-CIT SPECT imaging assessment of the rate of Parkinson's disease progression. *Neurology* 2001; 57: 2089–94.
- Marques JP, Kober T, Krueger G, van der Zwaag W, Van de Moortele PF, Gruetter R. MP2RAGE, a self bias-field corrected sequence for improved segmentation and T1-mapping at high field. *Neuroimage* 2010; 49: 1271–81.
- Martin WR, Wieler M, Gee M. Midbrain iron content in early Parkinson disease: a potential biomarker of disease status. *Neurology* 2008; 70: 1411–7.
- Matsusue E, Fujihara Y, Tanaka K, Aozasa Y, Shimoda M, Nakayasu H, et al. The utility of the combined use of (123)I-FP-CIT SPECT and neuromelanin MRI in differentiating Parkinson's disease from other parkinsonian syndromes. *Acta Radiol* 2019; 60: 230–8.
- Matsuura K, Maeda M, Tabei KI, Umino M, Kajikawa H, Satoh M, et al. A longitudinal study of neuromelanin-sensitive magnetic resonance imaging in Parkinson's disease. *Neurosci Lett* 2016; 633: 112–7.
- Mattis S. Dementia rating scale. Professional manual. Florida: Psychological Assessment Resources; 1988.
- Mattis S, Bellak L, Karasu TB. Mental Status Examination for Organic Mental Syndrome in the Elderly Patient. Geriatric psychiatry a handbook for psychiatrists and primary care physicians. New York: Grune & Stratton; 1976.
- Mazziotta J, Toga A, Evans A, Fox P, Lancaster J, Zilles K, et al. A probabilistic atlas and reference system for the human brain:

- international Consortium for Brain Mapping (ICBM). *Phil Trans R Soc Lond B* 2001a; 356: 1293–322.
- Mazziotta J, Toga A, Evans A, Fox P, Lancaster J, Zilles K, et al. A four-dimensional probabilistic atlas of the human brain. *J Am Med Assoc* 2001b; 8: 401–30.
- Mazziotta JC, Toga AW, Evans A, Fox P, Lancaster J. A probabilistic atlas of the human brain: theory and rationale for its development. *Neuroimage* 1995; 2: 89–101.
- McGeer PL, Itagaki S, Boyes BE, McGeer EG. Reactive microglia are positive for HLA-DR in the substantia nigra of Parkinson's and Alzheimer's disease brains. *Neurology* 1988; 38: 1285–91.
- Modat M, Ridgway GR, Taylor ZA, Lehmann M, Barnes J, Hawkes DJ, et al. Fast free-form deformation using graphics processing units. *Comput Methods Programs Biomed* 2010; 98: 278–84.
- Mogenson G, Jones D, Yim C. From motivation to action: functional interface between the limbic system and the motor system. *Prog Neurobiol* 1980; 14: 69–97.
- Montague PR, Dayan P, Sejnowski TJ. A framework for mesencephalic dopamine systems based on predictive Hebbian learning. *J Neurosci* 1996; 16: 1936–47.
- Mugler JP, Brookeman JR. Rapid three-dimensional T1-weighted magnetic resonance imaging with the MP-RAGE sequence. *J Magn Reson Imaging* 1991; 1: 561–7.
- Nandhagopal R, Kuramoto L, Schulzer M, Mak E, Cragg J, Lee CS, et al. Longitudinal progression of sporadic Parkinson's disease: a multi-tracer positron emission tomography study. *Brain* 2009; 132: 2970–9.
- Nasreddine ZS, Phillips NA, Bedirian V, Charbonneau S, Whitehead V, Collin I, et al. The Montreal Cognitive Assessment, MoCA: a brief screening tool for mild cognitive impairment. *J Am Geriatr Soc* 2005; 53: 695–9.
- Nauta WJH, Smith GP, Faull RLM, Domesick VB. Efferent connections and nigral afferents of the nucleus accumbens septi in the rat. *Neuroscience* 1978; 3: 385–401.
- Nichols TE, Holmes AP. Nonparametric permutation tests for functional neuroimaging: a primer with examples. *Hum Brain Mapp* 2002; 15: 1–25.
- Ofori E, Pasternak O, Planetta PJ, Li H, Burciu RG, Snyder AF, et al. Longitudinal changes in free-water within the substantia nigra of Parkinson's disease. *Brain* 2015; 138: 2322–31.
- Ohtsuka C, Sasaki M, Konno K, Koide M, Kato K, Takahashi J, et al. Changes in substantia nigra and locus coeruleus in patients with early-stage Parkinson's disease using neuromelanin-sensitive magnetic resonance imaging. *Neurosci Lett* 2013; 541: 93–8.
- Ourselin S, Roche A, Subsol G, Pennec X, Ayache N. Reconstructing a 3D structure from serial histological sections. *Image Vis Comput* 2001; 19: 25–31.
- Parkinson Study Group. Dopamine transporter brain imaging to assess the effects of pramipexole vs levodopa on Parkinson disease progression. *JAMA* 2002; 287: 1653–61.
- Pauli WM, Larsen T, Collette S, Tyszka JM, Seymour B, O'Doherty JP. Distinct contributions of ventromedial and dorsolateral subregions of the human substantia nigra to appetitive and aversive learning. *J Neurosci* 2015; 35: 14220–33.
- Pirker W, Holler I, Gerschlag W, Asenbaum S, Zettinig G, Brucke T. Measuring the rate of progression of Parkinson's disease over a 5-year period with beta-CIT SPECT. *Mov Disord* 2003; 18: 1266–72.
- Postuma RB, Iranzo A, Hu M, Hogl B, Boeve BF, Manni R, et al. Risk and predictors of dementia and parkinsonism in idiopathic REM sleep behaviour disorder: a multicentre study. *Brain* 2019; 142: 744–59.
- Prange S, Danaïla T, Laurencin C, Caire C, Metereau E, Merle H, et al. Age and time course of long-term motor and nonmotor complications in Parkinson disease. *Neurology* 2019; 92: e148–e60.
- Prasad S, Stezin A, Lenka A, George L, Saini J, Yadav R, et al. Three-dimensional neuromelanin-sensitive magnetic resonance imaging of the substantia nigra in Parkinson's disease. *Eur J Neurol* 2018; 25: 680–6.
- Pyatigorskaya N, Gaurav R, Arnaldi D, Leu-Semenescu S, Yahia-Cherif L, Valabregue R, et al. Magnetic resonance imaging biomarkers to assess substantia nigra damage in idiopathic rapid eye movement sleep behavior disorder. *Sleep* 2017; 40: 1–8. doi: 10.1093/sleep/zsx149.
- Pyatigorskaya N, Magnin B, Mongin M, Yahia-Cherif L, Valabregue R, Arnaldi D, et al. Comparative Study of MRI biomarkers in the substantia nigra to discriminate idiopathic Parkinson disease. *AJNR Am J Neuroradiol* 2018; 39: 1460–7.
- R Core Team. R: A language and environment for statistical computing. <https://www.R-project.org/>; 2017.
- Reimao S, Ferreira S, Nunes RG, Pita Lobo P, Neutel D, Abreu D, et al. Magnetic resonance correlation of iron content with neuromelanin in the substantia nigra of early-stage Parkinson's disease. *Eur J Neurol* 2016; 23: 368–74.
- Reimao S, Pita Lobo P, Neutel D, Guedes LC, Coelho M, Rosa MM, et al. Substantia nigra neuromelanin-magnetic resonance imaging differentiates essential tremor from Parkinson's disease. *Mov Disord* 2015; 30: 953–9.
- Rieu I, Martinez-Martin P, Pereira B, De Chazeron I, Verhagen Metman L, Jahanshahi M, et al. International validation of a behavioral scale in Parkinson's disease without dementia. *Mov Disord* 2015; 30: 705–13.
- Sasaki M, Shibata E, Tohyama K, Takahashi J, Otsuka K, Tsuchiya K, et al. Neuromelanin magnetic resonance imaging of locus coeruleus and substantia nigra in Parkinson's disease. *Neuroreport* 2006; 17: 1215–8.
- Scherfler C, Seppi K, Mair KJ, Donnemiller E, Virgolini I, Wenning GK, et al. Left hemispheric predominance of nigrostriatal dysfunction in Parkinson's disease. *Brain* 2012; 135: 3348–54.
- Schultz W, Dayan P, Montague PR. A neural substrate of prediction and reward. *Science* 1997; 275: 1593–9.
- Schwarz J, Storch A, Koch W, Pogarell O, Radau PE, Tatsch K. Loss of dopamine transporter binding in Parkinson's disease follows a single exponential rather than linear decline. *J Nucl Med* 2004; 45: 1694–7.
- Schwarz ST, Rittman T, Gontu V, Morgan PS, Bajaj N, Auer DP. T1-weighted MRI shows stage-dependent substantia nigra signal loss in Parkinson's disease. *Mov Disord* 2011; 26: 1633–8.
- Schwarz ST, Xing Y, Tomar P, Bajaj N, Auer DP. In vivo assessment of brainstem depigmentation in Parkinson disease: potential as a severity marker for multicenter studies. *Radiology* 2017; 283: 789–98.
- Simuni T, Siderowf A, Lasch S, Coffey CS, Caspell-Garcia C, Jennings D, et al. Longitudinal change of clinical and biological measures in early Parkinson's Disease: Parkinson's progression markers initiative cohort. *Mov Disord* 2018; 33: 771–82.
- Staffen W, Mair A, Unterrainer J, Trinka E, Ladurner G. Measuring the progression of idiopathic Parkinson's disease with [123I] beta-CIT SPECT. *J Neural Transm (Vienna)* 2000; 107: 543–52.
- Sulzer D, Cassidy C, Horga G, Kang UJ, Fahn S, Casella L, et al. Neuromelanin detection by magnetic resonance imaging (MRI) and its promise as a biomarker for Parkinson's disease. *NPJ Parkinsons Dis* 2018; 4: 11.
- Takahashi H, Watanabe Y, Tanaka H, Mihara M, Mochizuki H, Liu T, et al. Quantifying changes in nigrosomes using quantitative susceptibility mapping and neuromelanin imaging for the diagnosis of early-stage Parkinson's disease. *Br J Radiol* 2018a; 91: 20180037.
- Takahashi H, Watanabe Y, Tanaka H, Mihara M, Mochizuki H, Takahashi K, et al. Comprehensive MRI quantification of the substantia nigra pars compacta in Parkinson's disease. *Eur J Radiol* 2018b; 109: 48–56.
- Taniguchi D, Hatano T, Kamagata K, Okuzumi A, Oji Y, Mori A, et al. Neuromelanin imaging and midbrain volumetry in progressive supranuclear palsy and Parkinson's disease. *Mov Disord* 2018; 33: 1488–92.
- Wang J, Huang Z, Li Y, Ye F, Wang C, Zhang Y, et al. Neuromelanin-sensitive MRI of the substantia nigra: an imaging

- biomarker to differentiate essential tremor from tremor-dominant Parkinson's disease. *Parkinsonism Relat Disord* 2019; 58: 3–8.
- Wang J, Li Y, Huang Z, Wan W, Zhang Y, Wang C, et al. Neuromelanin-sensitive magnetic resonance imaging features of the substantia nigra and locus coeruleus in de novo Parkinson's disease and its phenotypes. *Eur J Neurol* 2018; 25: 949–e73.
- Xing Y, Sapuan A, Dineen RA, Auer DP. Life span pigmentation changes of the substantia nigra detected by neuromelanin-sensitive MRI. *Mov Disord* 2018; 33: 1792–9.
- Zaghloul KA, Blanco JA, Weidemann CT, McGill K, Jaggi JL, Baltuch GH, et al. Human substantia nigra neurons encode unexpected financial rewards. *Science* 2009; 323: 1496–9.
- Zecca L, Stroppolo A, Gatti A, Tampellini D, Toscani M, Gallorini M, et al. The role of iron and copper molecules in the neuronal vulnerability of locus coeruleus and substantia nigra during aging. *Proc Natl Acad Sci USA* 2004; 101: 9843–8.
- Zou J, Weng RH, Chen ZY, Wei XB, Wang R, Chen D, et al. Position Emission Tomography/Single-Photon Emission Tomography neuroimaging for detection of premotor Parkinson's disease. *CNS Neurosci Ther* 2016; 22: 167–77.